Optical and Quantum Electronics **30** *(1998) 861–879*

Interactions between one-dimensional quadratic soliton-like beams

R. SCHIEK, Y. BAEK*, G. STEGEMAN
C.R.E.O.L., University of Central Florida, 4000 Central Florida Blvd, Orlando 32816-2700, USA

W. SOHLER
Angewandte Physik, Universität-GH Paderborn, Warburger Strasse 100, D-33098 Paderborn, Germany

The interaction between two quadratic soliton-like beams was investigated for beams launched parallel to one another, and at small crossing angles. The experiments were performed in titanium in-diffused lithium niobate slab waveguides near a Type I phase-matching condition for second harmonic generation (SHG). Only beams at the fundamental frequency were launched and the second harmonic required for quadratic soliton formation was generated upon propagation into the waveguide. The results of the interaction were found to depend on the relative phase between the input fundamental beams, the net phase mismatch for SHG and on the beam crossing angle. Good agreement with numerical simulations of the different interactions was found. In general, the results of the interactions were similar to those found in saturable Kerr-like media.

1. Introduction

Generically spatial solitons are beams which propagate without spreading (diffraction) in one or more transverse beam dimensions due to the existence of some self-focusing mechanism [1–3]. There has been a proliferation of such spatial solitons demonstrated, primarily over the last 5–10 years, including solitons in Kerr, saturable Kerr, photorefractive and quadratically non-linear media [4–13]. Most popular by far have been solitons based on non-linear mechanisms which lead to an optically induced local increase or decrease in the refractive index [4–11]. The arresting of spatial diffraction by some non-linear self-focusing mechanism has been investigated in both one dimension (1D, beams in slab waveguides) and two dimensions (2D, in bulk media). In analogy to temporal solitons in glass fibres (Kerr media), the earliest experiments utilized Kerr ($\Delta n(I) = n_2 I$, where I is the local intensity) and saturable Kerr ($\Delta n(I) \rightarrow \Delta n_{\text{sat}}$ as $I \rightarrow \infty$) non-linear media to demonstrate both bright and dark spatial solitons [4–9]. About five years ago it was proposed that the photorefractive effect in electro-optic media could be used to form spatial solitons and indeed a large number of such solitons have now been reported in both 1D and 2D [10, 11].

*Current address: Dept. of Physics, Washington State University, Pullman, WA 99164-2814, USA.

0306–8919

A different type of spatial soliton was proposed in the 1970s by Karamzin and Sukhorukov [14, 15]. The self-focusing action required to counteract diffraction was provided by the strong interaction between waves at two or three different frequencies due to the second order non-linearity $\chi^{(2)}$. The coupled waves form a multi-component 'quadratic' soliton, with all of the frequency components travelling together [14–23]. The theoretical aspects of such quadratic solitons have been investigated intensively in the last five years, and many of their properties including their multifrequency structure, stability, etc. have been understood [14–23]. These solitons have been observed in both 1D (Ti:in-diffused $LiNbO_3$ slab waveguides) and 2D (bulk KTP crystals), in both Type I and II phase-matching geometries [12, 13]. Furthermore, many of the soliton properties including the connection with modulational instabilities, beam steering, relative strength of the interacting waves etc. have been studied experimentally [24–27].

Faced now with this large diversity of solitons, the question is what properties do they have in common besides propagation without diffraction spreading [1–3]. Interactions and collisions are effects where there is some diversity in soliton properties [28–32]. It has been known for some time now that single polarization solitons in Kerr media always pass through each other with some lateral deflection, independent of the details of the interaction geometry. (Only under very special circumstances, two orthogonally polarized Kerr solitons colliding at small angles can fuse together to produce a dual polarization stable soliton called a Manakov soliton [33].) On the other hand, it has been clearly established that other types of spatial solitons which rely on index changes for trapping, for example photorefractive solitons, solitons in saturable media etc., can fuse together under appropriate interaction conditions [31, 32]. The collision behaviour is determined by the type of soliton. Solitons which are modelled as solutions of integrable equations do not fuse in a collision while the non-conservation of the soliton number in an interaction is a property of solutions of non-integrable systems [1–3]. In order to distinguish soliton solutions of both systems the self-trapped beams in non-integrable systems are frequently (and more precisely) called solitary or soliton-like waves.

The multifrequency nature of quadratic solitary waves makes them quite unique in the optical soliton family [12–27, 34]. For example, the properties of the solitons depend strongly on the phase mismatch. For progressively larger positive phase mismatch, the harmonic component becomes progressively smaller and the solitons resemble Kerr solitons (integrable system) [20, 21]. On the other hand, near phase matching and for negative phase mismatch, the quadratic soliton properties are quite different (non-integrable system). Thus the results of their interactions would be expected to depend on the phase mismatch, and the features of interactions of both soliton types can be studied with quadratic solitons. Numerical calculations have established for the Type I case that quadratic solitons can penetrate each other or fuse when they interact, and that their collisional properties depend on the relative phase between the solitons [17, 35–38]. We have experimentally investigated the interaction of quadratic soliton-like beams in planar $LiNbO_3$ waveguides under different Type I phase-matching conditions [39]. In our case, we launched only the fundamental component and relied on the usual second harmonic generation (SHG) process to produce the harmonic component of the right phase needed for beam locking into a quadratic soliton. As a result an interaction starts even before the soliton is completely formed which influences to some extent our results. Some of the interesting results have already been published in summary form in letter format and here we give more of the details and more complete data.

This paper is structured as follows. The next section deals with some of the relevant properties of quadratic spatial solitons and our excitation conditions. The details of the experiment and sample are presented in Section 3. Results for the launching of parallel fundamental beams are discussed in Section 4, in the limits of both large and small phase-mismatch. The last experimental section deals with the collisions of solitons launched in crossing geometries. The main features of this work are summarized in Section 6.

2. Theoretical considerations

In general, numerical techniques are needed to estimate the properties of quadratic solitons for arbitrary values of the phase mismatch. Many of the fundamental properties of quadratic solitons, especially in the simplest 1D case with Type I phase-matching are now well established [34]. When spatial diffraction is included, the SHG coupled mode equations describe the fundamental and harmonic components, how they evolve with distance, and in the steady state limit they give the stationary quadratic solitons. Consider a slab waveguide (1D) with a geometry corresponding to that used experimentally, i.e. propagation along the x-axis in the x–z plane so that the guided wave confinement occurs along the y-axis. For the simplest 1D case of Type I phase matching, the z (diffraction direction) and x (propagation direction) dependence of the interacting fundamental and harmonic fields can be written respectively as:

$$E_1(\vec{r},t)=\tfrac{1}{2}a_1(x,z)\,e_1(y)\exp[\mathrm{i}(\omega t-k_1x)]+\mathrm{cc}\quad E_2(\vec{r},t)=\tfrac{1}{2}a_2(x,z)\,e_2(y)\exp[\mathrm{i}(2\omega t-k_2x)]+\mathrm{cc} \tag{1}$$

where the subscript 1 identifies parameters at the fundamental frequency ω, and the subscript 2 refers to the second harmonic (2ω). The complex amplitudes $a_i(x,z)$ can change due to spatial diffraction and/or the energy exchange due to the coupling between the fundamental and harmonic fields which occurs during harmonic generation. The corresponding coupled mode equations are:

$$\begin{aligned} -2\mathrm{i}k_1\frac{\partial}{\partial x}a_1(x,z)+\frac{\partial^2}{\partial z^2}a_1(x,z)&=-2k_1\Gamma a_1^*(x,z)a_2(x,z)\,\exp[\mathrm{i}\Delta kx]\\ -2\mathrm{i}k_2\frac{\partial}{\partial x}a_2(x,z)+\frac{\partial^2}{\partial z^2}a_2(x,z)&=-2k_2\Gamma a_1^2(x,z)\,\exp[-\mathrm{i}\Delta kx]\end{aligned} \tag{2}$$

Here $\Delta k = 2k_1 - k_2$ is the linear wavevector mismatch (and ΔkL the phase mismatch) and $\Gamma = \omega K^{(2)}2\chi^{(2)}/4p_0$, the non-linear coupling coefficient, is proportional to the second order susceptibility $\chi^{(2)}$ for the appropriate material symmetry class and field geometry. It includes the 'overlap integral' $K^{(2)}$ of the fundamental and harmonic guided wave fields. Note that walk-off between the two beams is absent for propagation in the present case, i.e. propagation and field polarization along the principal optical axes of a crystal.

Stationary solutions, i.e. ones in which the spatial profile and peak amplitude of the fundamental and harmonic components do not change with propagation distance, are obtained by setting the $\partial/\partial x$ derivatives as pure imaginary constants. Among the whole family of solitons there is one specific value of the phase mismatch ΔkL for which an exact analytical solution is possible, and this predicts fields whose transverse profiles (along the z-axis) both vary as $\mathrm{sech}^2(s)(s \propto z)$ [14, 15, 17]. There is another limit in which an approximate analytical field distribution is known. That is, when $\Delta kL \to \infty$ the fundamental field closely resembles a Kerr soliton because the second harmonic field contribution

becomes vanishingly small, i.e. $a_1 \propto \mathrm{sech}(s)$ and $a_2 \propto \mathrm{sech}^2(s)$ with $|a_1|^2 \gg |a_2|^2$ [40, 41]. This makes it clear that the field structure of the soliton depends strongly on the phase mismatch, and hence it is expected that the nature of soliton interaction will also depend on the phase mismatch ΔkL.

The interaction between two quadratic solitons was investigated with numerical techniques to simulate the behaviour for various geometries, relative fundamental phase differences $\Delta\phi$ at the input, and phase mismatches (ΔkL). It proves convenient to model the interaction with a coupled mode theory for spatial Fourier spectra which allows the non-uniform wavevector distribution in the sample (discussed later) and the wavevector spectrum associated with focusing along the diffraction coordinate (z) to be handled conveniently and with minimal approximations. The z-dependence of the electric field amplitude $\hat{E}_i = e_i(y)a_i(x,z)\exp(-\mathrm{i}\beta_i x)$ at every point x along the waveguide is expanded as spatial Fourier integrals in the form $\hat{E}_i(x,y,z) = [e_i(y)/2\pi]\int \mathrm{d}\beta_z\, A_i(x,\beta_z)\exp[\mathrm{i}\beta_z z]$. In this formalism, the up- and down-conversion processes are described by the Fourier transformed coupled mode equations of the form [42]

$$\begin{aligned}
\frac{\mathrm{d}}{\mathrm{d}x}A_1(\beta_z) + \mathrm{i}\beta_{1x}A_1(\beta_z) &= -\mathrm{i}\frac{\omega_1 K^{(2)} 2\chi^{(2)}\beta_1}{8\pi p_0 \beta_{1x}}\int \mathrm{d}\beta'_z\, A_2(\beta_z-\beta'_z)A_1^*(-\beta'_z)\\
\frac{\mathrm{d}}{\mathrm{d}x}A_2(\beta_z) + \mathrm{i}\beta_{2x}A_2(\beta_z) &= -\mathrm{i}\frac{\omega_1 K^{(2)} 2\chi^{(2)}\beta_2}{8\pi p_0 \beta_{2x}}\int \mathrm{d}\beta'_z\, A_1(\beta_z-\beta'_z)A_1(\beta'_z)
\end{aligned} \tag{3}$$

Here the normalized modal electric and magnetic field distributions are given by $e_i(y)$ and $h_i(y)$ respectively and $i = 1, 2$ identify the fundamental and harmonic beams. β_z is the spatial angular frequency, the $\beta_{ix} = [\beta_i^2 - \beta_{iz}^2]^{1/2}$ are the x-components of the mode propagation constants β_i, and p_0 is the normalized mode power per unit film width ($\mathrm{W\,m^{-1}}$). $K^{(2)} = \int \mathrm{d}y\, e_1^2(y)e_2^*(y)$ is the overlap integral which takes into account the different transverse electric field profiles of the interacting guided modes.

The results of the simulations based on Equations 3 are summarized in the collage of Figs. 1–4. Note that in this case the stationary soliton is launched numerically, i.e. the input contains both frequency components with field profiles, amplitudes and phases appropriate to a quadratic soliton [43]. For inputs launched parallel to one another and zero phase difference ($\Delta\phi = 0$), the interaction is attractive. Far from phase matching ($\Delta kL = 19\pi$, Fig. 1) where the quadratic solitons resemble Kerr solitons (second harmonic power $<3\%$ of the total power), the interaction in its early stages of evolution is very similar to that for Kerr solitons [30]. The solitons periodically coalesce and separate preserving the number of solitons as two. However, the spatial period between successive beam collapses, becomes progressively smaller with distance and eventually the beams fuse (not shown in Fig. 1) because finally the interacting quadratic solitons are only a good approximation to, but not truly, solutions of an integrable system. Close to phase matching ($\Delta kL = 1.36\pi$) the violation of the conservation law for the soliton number in the interaction of quadratic solitons is detectable already in the first stage of the interaction. The beams fuse immediately, and then the peak intensity and spatial width oscillate periodically with distance [36]. The beams shed energy and the oscillations damp out with distance, eventually yielding a stationary soliton. Note that the excess radiation emitted to the side is larger the smaller the value of ΔkL, i.e. the closer to phase matching. For all other relative phase angles the interaction is repulsive after a $\Delta\phi$-dependent propagation distance with the trend to larger radiative losses with decreasing positive phase mismatch

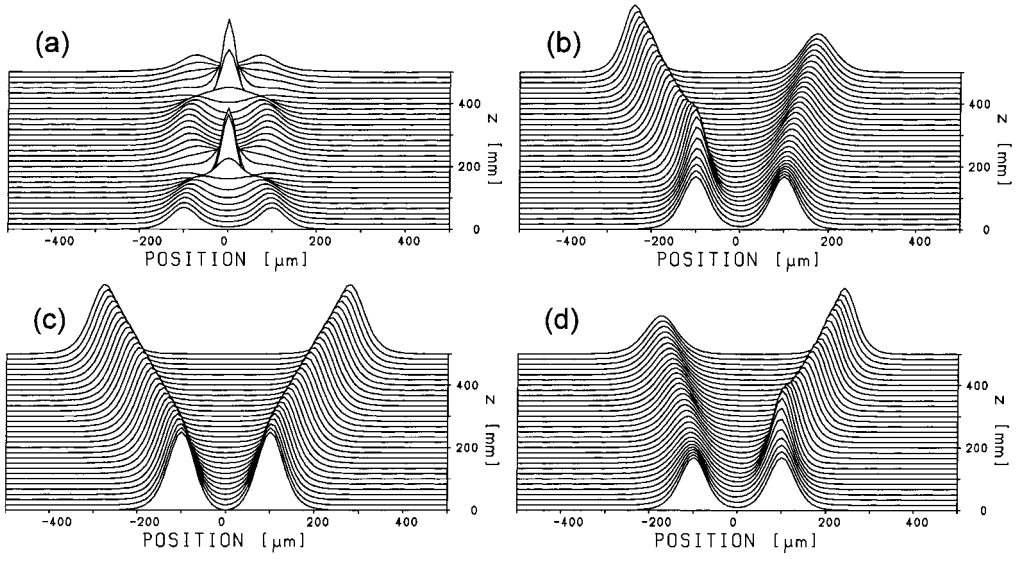

Figure 1 Interaction between two stationary quadratic solitons launched parallel to each other for $\Delta kL = 19\pi$ ($L = 47$ mm). The initial relative phase between the solitons is (a) 0, (b) $\pi/2$, (c) π and (d) $3\pi/2$.

in each case. Finally, away from $\Delta\phi = 0$ or π, one soliton grows at the expense of the other with the power exchange increasing with decreasing phase mismatch.

The numerical results for the crossing geometries, shown in Figures 3 and 4, are qualitatively similar to the parallel launch case with respect to large versus small phase-mismatch, power exchange, trends in radiation losses, etc. The repulsive beam deflection

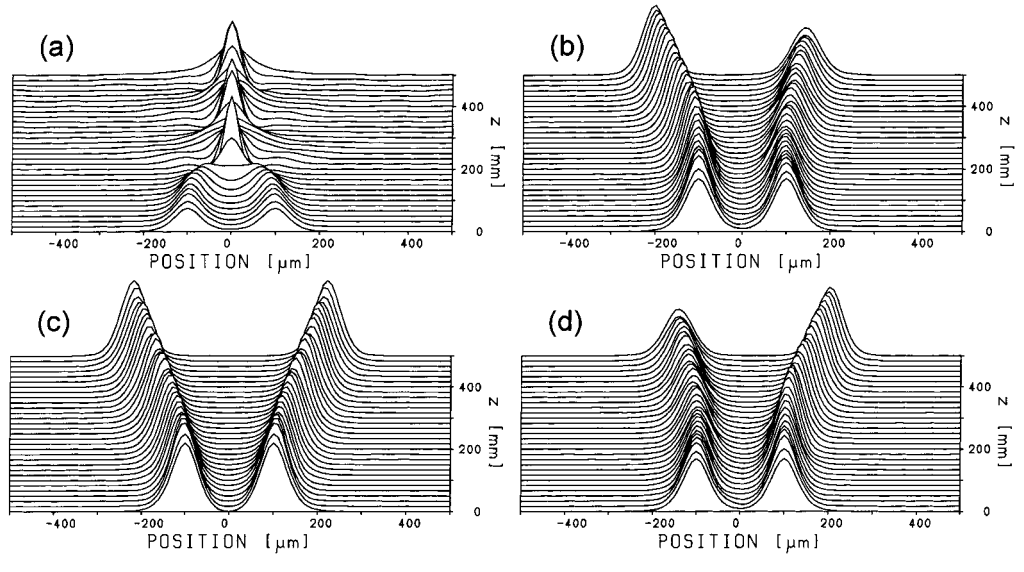

Figure 2 Interaction between two stationary quadratic solitons launched parallel to each other for $\Delta kL = 1.36\pi$ ($L = 47$ mm). The initial relative phase between the solitons is (a) 0, (b) $\pi/2$, (c) π and (d) $3\pi/2$.

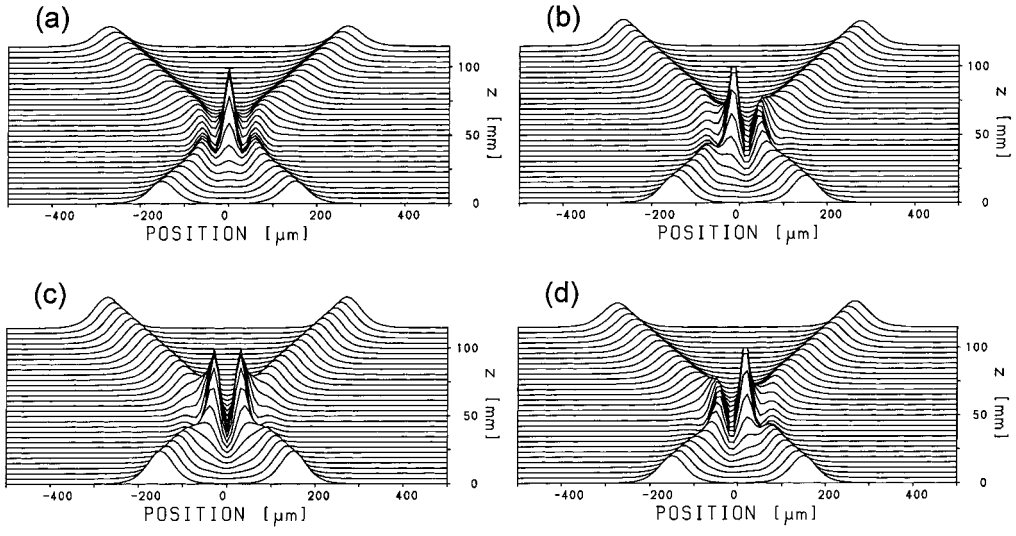

Figure 3 Interaction between two stationary quadratic solitons launched at a crossing angle of 0.4° for $\Delta kL = 19\pi$ ($L = 47$ mm). The initial relative phase between the solitons is (a) 0, (b) $\pi/2$, (c) π and (d) $3\pi/2$.

with negligible energy transfer for a large phase mismatch resembles a Kerr soliton crossing.

The attractive crossing with energy exchange and the fusion for small $\Delta\phi$ are characteristic for quadratic solitons at a smaller phase mismatch.

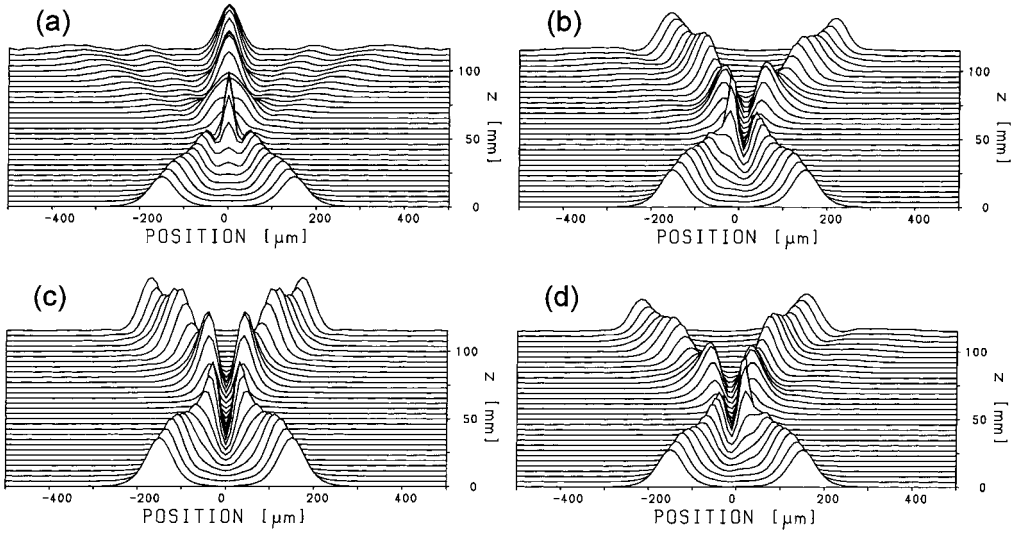

Figure 4 Interaction between two stationary quadratic solitons launched at a crossing angle of 0.4° for $\Delta kL = 1.36\pi$ ($L = 47$ mm). The initial relative phase between the solitons is (a) 0, (b) $\pi/2$, (c) π and (d) $3\pi/2$.

3. Experimental aspects

We have previously reported the generation of 1D quadratic solitons propagating along the x-axis of Y-cut, planar, Ti:in-diffused $LiNbO_3$ waveguides near the phase-matching conditions for Type I SHG at 1320 nm [12]. For this geometry, $\chi^{(2)} = \varepsilon_0(-5.6\,\mathrm{pm\,V^{-1}})$. The in-diffusion of a 55 nm thick titanium layer through the Y-cut surface at 1060°C for 9 h yielded a low loss one-dimensional waveguide which guides one TM mode (y-polarized) at $\lambda_1 = 1320\,\mathrm{nm}$ and three second harmonic TE modes (z-polarized) at $\lambda_2 = 660\,\mathrm{nm}$. The change in the refractive index profile mirrors the Ti concentration which decays with distance into the sample. This depth dependence of the refractive index provided the guided mode confinement along the y-axis. Losses of 0.17 and $0.35\,\mathrm{dB\,cm^{-1}}$ were found for the $TM_0(\omega)$ and $TE(2\omega)$ modes respectively. The end faces of the $L = 47\,\mathrm{mm}$ long sample were polished for end-fire coupling with the output surface tilted at 4.5° to prevent longitudinal cavity resonances. The details of the waveguide fabrication, characterization etc. can be found in [44]. The same sample was used in this work.

The apparatus used for exciting the quadratic solitons and observing the results of their interactions is shown in Fig. 5. The measurements were done with a train of pulses with 90 ps FWHM (full width at half maximum) and a repetition rate of 500 Hz, using a Nd:YAG Q-switched, mode-locked pulsed laser (76 MHz) and an electro-optic single pulse extractor. The intensity profile measurements of the waveguide output were averaged over many shots with a camera and were corrected for the (very weak) background light (measured separately) due to leakage of the Q-switched, mode-locked pulse envelope through the pulse slicer. There are two separate arms for the input beams, one for each soliton. A combination of optical elements was used to generate two separate, equi-power beams, one of which was delayed relative to the other to produce a well-defined relative phase difference at the sample input. Although this allows a great deal of control over each input, it also means that the input pulses need to be carefully synchronized in time. Cylindrical lenses were used to focus elliptically shaped beams with a horizontal spot size of 70 μm FWHM onto the sample input facet. The output from the planar sample (approximately three diffraction lengths long) was focused onto a vidicon camera for display and analysis.

In order to generate spatial solitary waves via the cascaded non-linearity, SHG was implemented from the $TM_0(\omega)$ to the $TE_1(2\omega)$ mode which is phase matched around 335.5°C for our material, geometry and wavelength. This mode combination optimizes the overlap integral in these in-diffused waveguides. The mutual beam trapping occurs in the

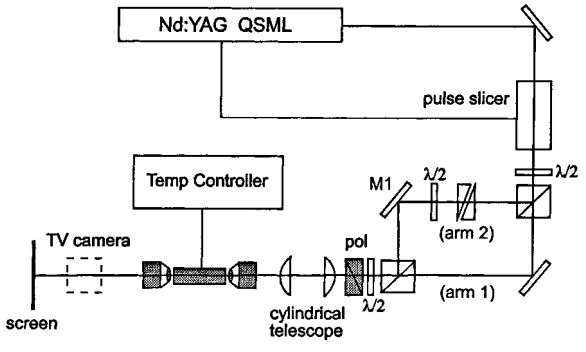

Figure 5 Experimental set-up for the investigation of quadratic soliton interactions in 1D.

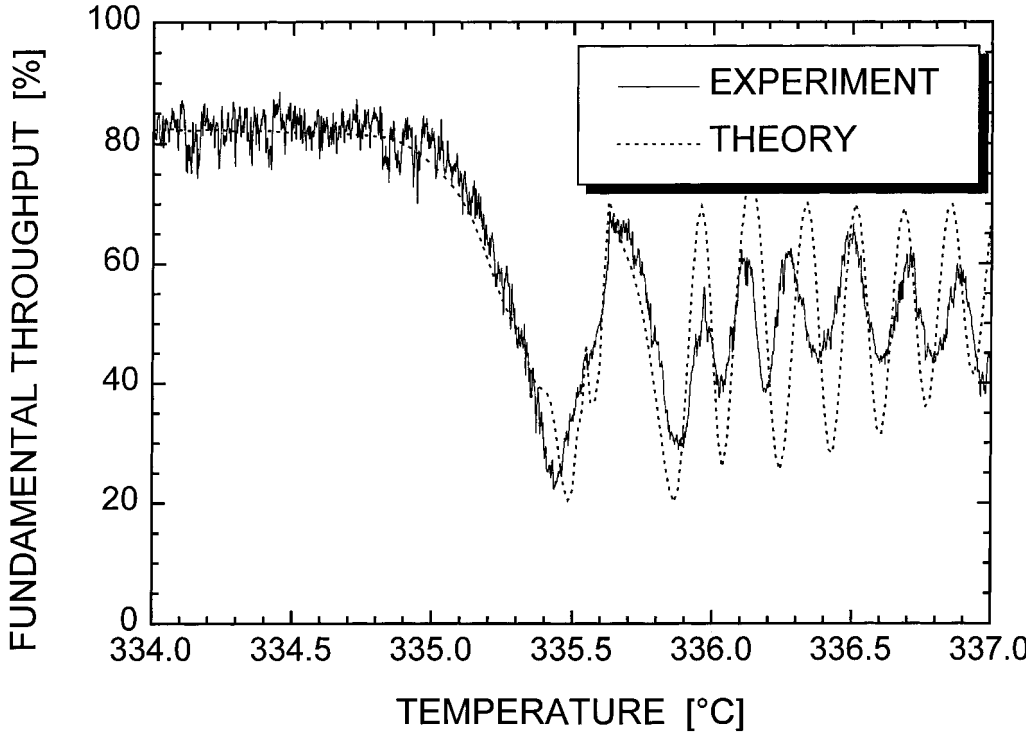

Figure 6 The fundamental beam throughput versus sample temperature as measured in the middle of the waveguide for a peak input power of $P_{IN} = 1.5\,kW$.

plane of the waveguide, i.e. along the z-axis. For phase-matching purposes the crystal was placed in an oven with temperature controlled to a stability of ± 25 mK. The resulting sample temperature distribution is nearly uniform in the centre of the waveguide, but drops a few degrees near the oven windows, i.e. the resulting wavevector mismatch varies with distance along the waveguide [45]. This leads to a very asymmetric SHG (and fundamental depletion) response, as shown in Fig. 6 [46]. In this work the solitons were generated both far from phase matching as well as close to phase matching.

Fortunately the low fundamental depletion region for $T < 335.2°C$ corresponds to a large positive phase mismatch allowing that limit to be explored experimentally very well. Although the complex wavevector mismatch distribution complicated the investigation of the quadratic soliton collisions, the solitons were still easily excited with less than 20% fundamental depletion at a positive phase mismatch up to about $\Delta kL \simeq 6\pi$ at $T = 335.2°C$ (as measured at the centre of the oven). An example of the output beam profiles for $\Delta kL \simeq 10\pi$ at $T = 334.9°C$ is shown in Fig. 7 in which the beam profile is unchanged to within10% for input powers above 1 kW (up to our maximum available power of 8 kW). Because the SH component of the solitons is small (<10%) relative to the fundamental for this large a detuning, the quadratic solitons resembled Kerr solitons based on $\chi^{(3)}$.

The experiments close to phase matching were performed in the range $-2.6\pi < \Delta kL < 2.6\pi$ of the low power phase mismatch which corresponds to the tem-

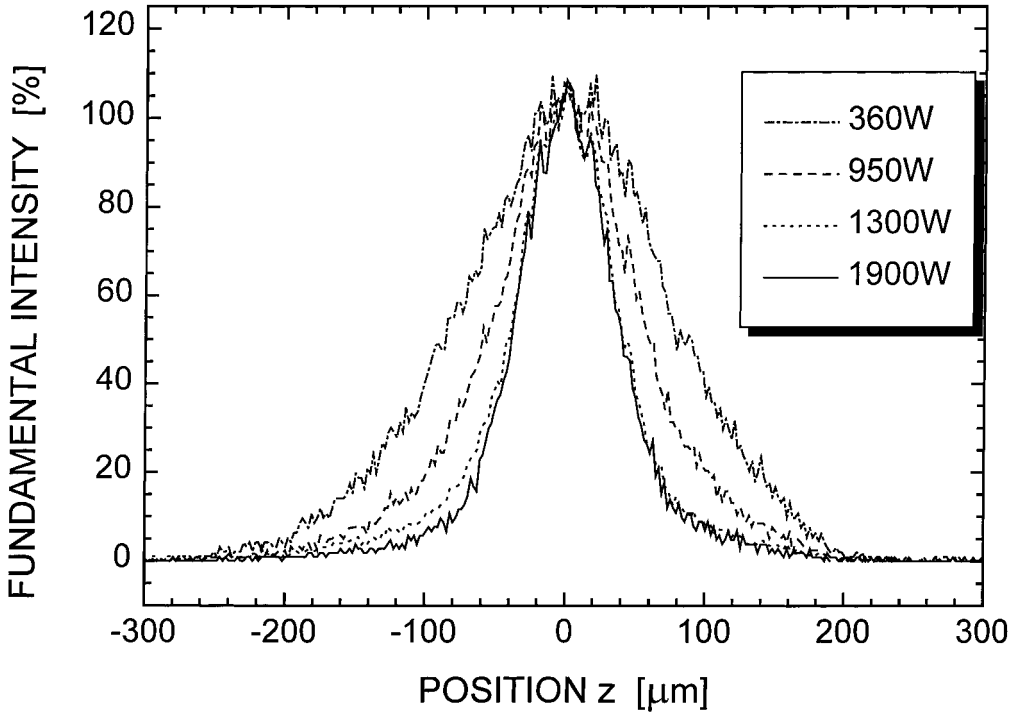

Figure 7 Power dependence of the output beam (intensity) profile of the fundamental for $\Delta kL \simeq 10\pi$, Temperature $T = 334.9°C$.

perature range from 335.9 to 335.5°C. In this range the soliton-like beam contains $\sim 50\%$ of the harmonic component and the depletion of the fundamental is significant. It falls in a region where the harmonic content (and the effective focusing non-linearity) is very sensitive to temperature and wavevector distribution. Operating close to phase match and in the negative phase-matching region, the low power phase-matching conditions are seriously detuned by non-linear phase shifts, and the exact form of the solitons becomes even more sensitive to the experimental conditions [46]. This extreme sensitivity of the results of the interactions was actually observed experimentally, i.e. small changes in the conditions (particularly temperature) produced large changes in the output beams observed. Our lack of knowledge of the exact wavevector non-uniformity prevented us from performing very well fitting simulations for comparison to experiment in this region.

In our experiments, the harmonic components of the quadratic solitons are generated from the input fundamental frequency beams during propagation of the fundamental into the waveguide. It is now well established that this approach leads asymptotically with propagation distance to quadratic solitons [12, 13, 40, 47, 48]. In the soliton's evolutionary stage this leads to radiation-like fields which, with the phase coherence length used, result in periodic oscillations of the intensity which decay with distance. The smaller the harmonic field component associated with the soliton, or the closer the input parameters are to a stationary soliton, the smaller the oscillations and the better the input

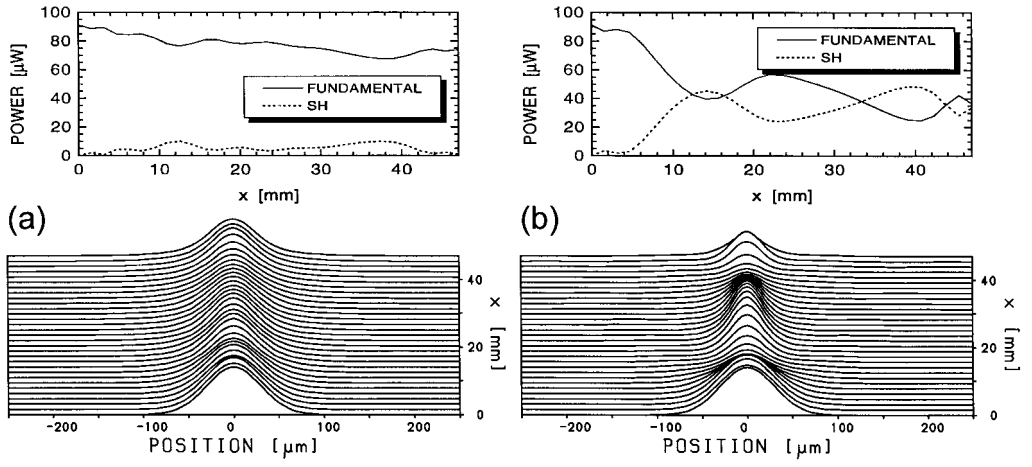

Figure 8 Simulated spatial evolution towards a quadratic soliton when only the fundamental is excited at the input (a) $T = 334.8°C, \Delta kL \simeq 11\pi, P_{IN} = 1.9\,kW$, (b) $T = 335.45°C, \Delta kL \simeq 3.2\pi, P_{IN} = 1.9\,kW$. The diagrams show the time averaged power in the fundamental and the second harmonic along the propagation.

field approximates a quadratic soliton. Simulations showing two examples of the evolution of a quadratic soliton from the launch of only a fundamental Gaussian input spot are shown in Fig. 8. The simulations take into account the details of the experimental conditions, like temperature profile, double refraction, walk-off, losses, pulsed input etc. Due to the non-uniform wavevector mismatch profile along the waveguide and the waveguide losses the oscillations are smoothed out. However, it is obvious that the lack of second harmonic seeding initiates strong oscillating perturbations in the solitons for decreasing phase mismatch.

Because our sample is too short for the solitons near phase matching to evolve into the stationary final state, it is these soliton-like, not yet stationary, quadratic soliton beams that we use in our experiments.

4. Interactions between parallel beams

In the experiments, two y-polarized (TM modes) fundamental beams, each 70 μm FWHM wide with a peak input power of 1.9 kW, were launched parallel to each other at a centre-to-centre separation of 110 μm. The transverse (along the z-axis) profiles of the input and output beams when each input was excited individually are shown in Fig. 9. Beam diffraction occurs at large phase mismatch at $T = 331°C$ whereas for increasing cascaded non-linearity (near phase matching) the solitons are formed. The beam widths and shapes of the input and output beams are the same for the Kerr-like quadratic solitons at $T = 334.8°C$. The missing energy in the fundamental output at $T = 335.7°C$ was converted into the second harmonic component of the quadratic soliton. The interaction is initiated by the overlap of the tails of the soliton-like beams as they evolve. The experimental results and the corresponding simulations at $\Delta kL \simeq 10\pi$ ($T = 334.9°C$) are shown in Fig. 10. The main features of Kerr-like quadratic soliton interactions far from phase match were observed. For example, the repulsion is evident for $\pi/2 < \Delta\phi < 3\pi/2$, as well as the power exchange between the solitons. For example, a 20% increase in the peak separation was obtained for $\Delta\phi = \pi$. Our sample was not long enough to observe the

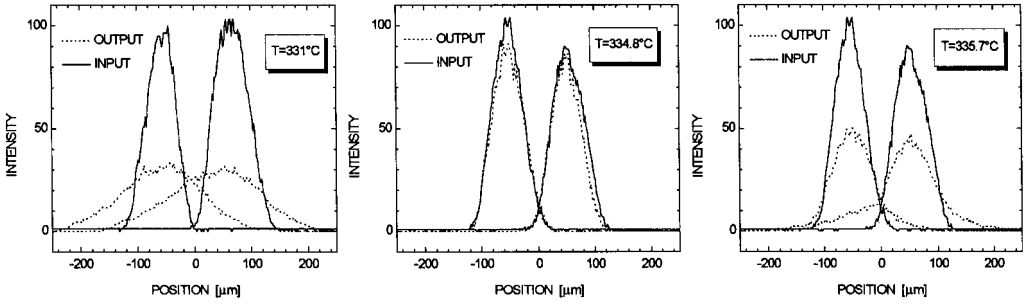

Figure 9 Transverse beam profiles at the input and the output for the two fundamental beams (launched separately) for different temperatures and phase mismatch. The peak input power in one arm is 1.9 kW.

soliton repulsion for a phase difference in the range $0 < |\Delta\phi| < \pi/2$ for which repulsion is expected only after a longer propagation distance. For $\Delta\phi = 0$ the simulations show that the output corresponds to the first merging of the beams and therefore that is also consistent with the interactions between in-phase stationary solitons. Numerical simulations of the soliton interaction in our waveguide show results very similar to those presented in Fig. 1, with only minor changes due to the SHG near the input. The theoretical interaction results in this large phase-mismatch region can be perfectly approximated with simulations of Kerr soliton interactions.

Closer to phase match, for $T = 335.7°C$, it is clear from the experimental results and the corresponding simulations in Fig. 11 that the interaction result is not as well developed as found previously for $\Delta kL \simeq 10\pi$, although the principal behaviour remains the same. The closer the second harmonic generation is to phase matching, the larger the harmonic component needed for a quadratic soliton and the longer the propagation distance into the sample required to generate sufficient harmonic when only the fundamental beam is launched. The beams oscillate strongly in intensity and the resulting interference pattern modulates the soliton interaction. The other notable difference compared to the $\Delta kL \simeq 10\pi$ case is the large amount of radiation fields present. Our samples are too short to verify that the solitons near phase matching fuse after the first (and observed) merging while the solitons at $T = 334.9°C$ should repulse again. It is interesting that the strong SHG oscillations due to the missing second harmonic seeding in our beams only modulate the soliton interaction but do not destroy the principal behaviour of the interaction. Compare for example the simulation results of the soliton repulsion with and without seeding in Fig. 12 and 2.

Although the agreement with the simulations is reasonable, there are some interesting differences between the simulations and the experimental data. As shown in [49], for fundamental beam launching conditions, the detailed nature of the output depends critically on the beam separation at the input. Furthermore, our simulations have shown that the output of the interaction is very sensitive to the details of the temperature (and hence wavevector mismatch) profile along the propagation axis. We have not yet measured this profile directly and only estimate it from the SHG tuning curves which were taken by ramping the temperature with a speed of $36\,K\,h^{-1}$ [12]. However, the soliton experiments were done at fixed oven temperatures at which the temperature, and hence the wavevector mismatch distribution, deviates from our estimates. Another uncertainty arises from the fact that the input beams may be slightly focused or defocused when entering the waveguide. Temperature and laser power fluctuations influence the relative

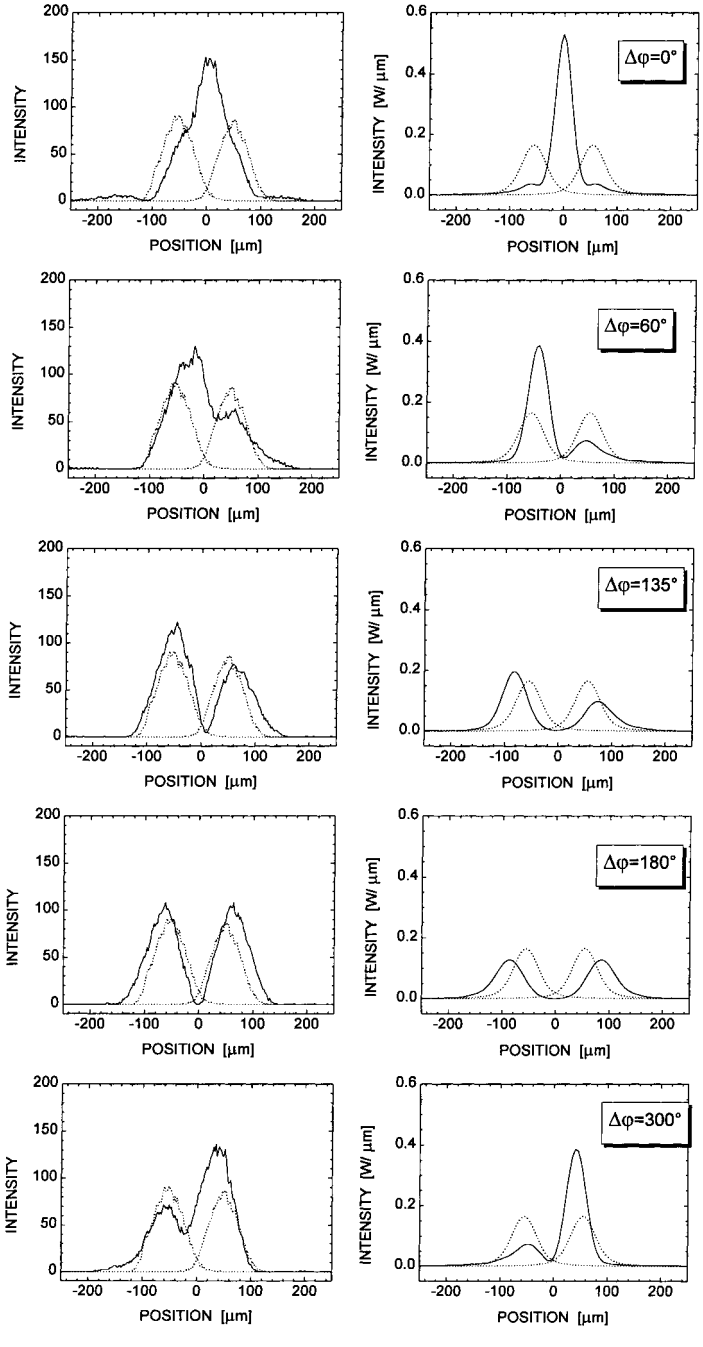

Figure 10 Beam profiles at the waveguide output for two fundamental beams launched in parallel with different relative phase angles. The detuning from phase match is $\Delta kL \simeq 10\pi$ at $T = 334.9°C$. The dotted lines show the output beams when they are launched separately (experiment: left hand side, theory: right hand side).

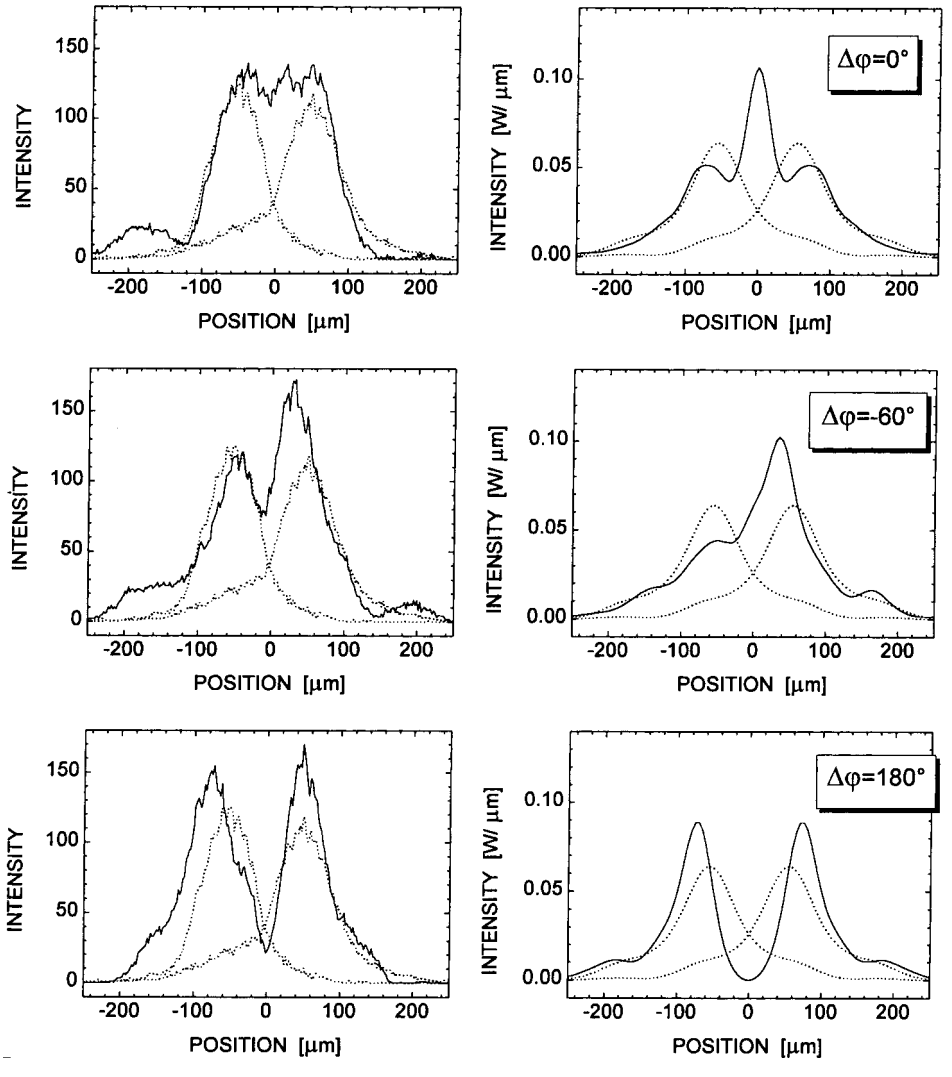

Figure 11 Beam profiles at the waveguide output for two fundamental beams launched in parallel with different relative phase angles. The detuning from phase match is $\Delta kL \simeq -0.2\pi$ at a temperature of 335.7°C. The dotted lines show the output beams when they are launched separately (experiment: left hand side, theory: right hand side).

strength and position of the output beams. A non-perfect temporal overlap of the pulses yields beam interaction patterns with reduced contrast between the principal features. Finally, the crystal input face may not be cut exactly orthogonal to the x-axis which would introduce the asymmetries observed experimentally. We have seen evidence for this problem in previous experiments [12]. All of the above mentioned uncertainties associated with our experimental accuracy alone modify the results only by a few per cent. However, together they cause the differences between the experimental and the theoretical results.

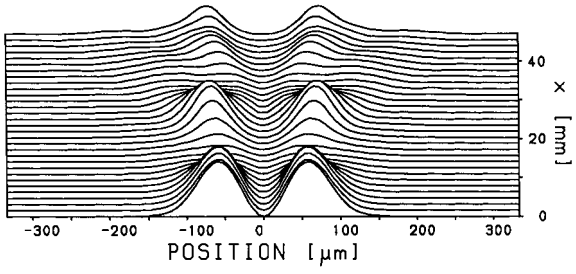

Figure 12 Simulation of the observed soliton repulsion of two parallel launched beams in phase at $T = 335.7°C$ without second harmonic seeding ($\Delta kL = -0.2\pi$).

5. Interactions between beams launched to cross inside the sample

In the second geometry, the two fundamental beams, initially separated by 100 μm, were launched at a collision angle inside the crystal of 0.4° in order to investigate the collision of two crossing solitons. Again, the behaviour at different values of the phase mismatch was studied. The results of the experiments and the corresponding simulations are shown in Figs. 13–15.

Based on the simulations, the crossing angle was chosen so that the beams would fuse for $\Delta kL < 3\pi$, but pass through each other for $\Delta kL \simeq 10\pi$. Figure 13 shows the output beam profiles at large phase mismatch ($T = 335.0°C, \Delta kL \simeq 9\pi$). For $\Delta\phi = 0$ the two beams passed through each other and are separating at the end of the sample. The wings of the solitons are indicative of some radiation generated during the interaction. In the case of out-of-phase ($\Delta\phi = \pi$) launching, similar behaviour was observed although the background seems reduced. Furthermore, for $\Delta\phi = \pi/2$ or $3\pi/2$, a small energy transfer between the solitons was observed. For all initial phase differences $\Delta\phi$ the output beams attract each other. The attraction is stronger in the in-phase case. The results were in excellent agreement with the numerical simulations for this large phase-mismatch case. They resemble Kerr soliton crossings except for the energy exchange and the existence of soliton attraction instead of repulsion obtained with Kerr solitons. This occurs because we could not operate far enough from phase matching to have true Kerr-like solitons and we observed already the tendency to attract and finally fuse in the crossing which will be discussed next.

For small phase mismatch, i.e. $\Delta kL \simeq 2.6\pi$ at 335.5°C, the experimental results are in good agreement with the simulations. For $\Delta\phi = 0$, the two beams fuse and narrow into a single soliton of higher peak intensity than the 'input' solitons. It is clear that for all relative phase angles, a great deal of the incident electromagnetic energy is radiated away, partially underlying the soliton beams and complicating the interaction. At a further reduced phase mismatch of -2.4π at 335.9°C the crossing behaviour shown in Fig. 15 did not principally change from that shown in Fig. 14 and only the power in the fundamental is reduced due to stronger SHG.

6. Summary

The interactions between quadratic soliton-like beams have been investigated for Type I SHG phase matching in planar $LiNbO_3$ waveguides (one-dimensional case). Two geometries were studied, one in which the beams were launched parallel to one another, and the second at relative angles chosen so that the beams would 'cross' before the middle of the sample. In addition, experiments were performed for different values of phase mismatch for the SHG interaction, between $\Delta kL \simeq 10\pi$ and -2π. Overall, the results agreed well

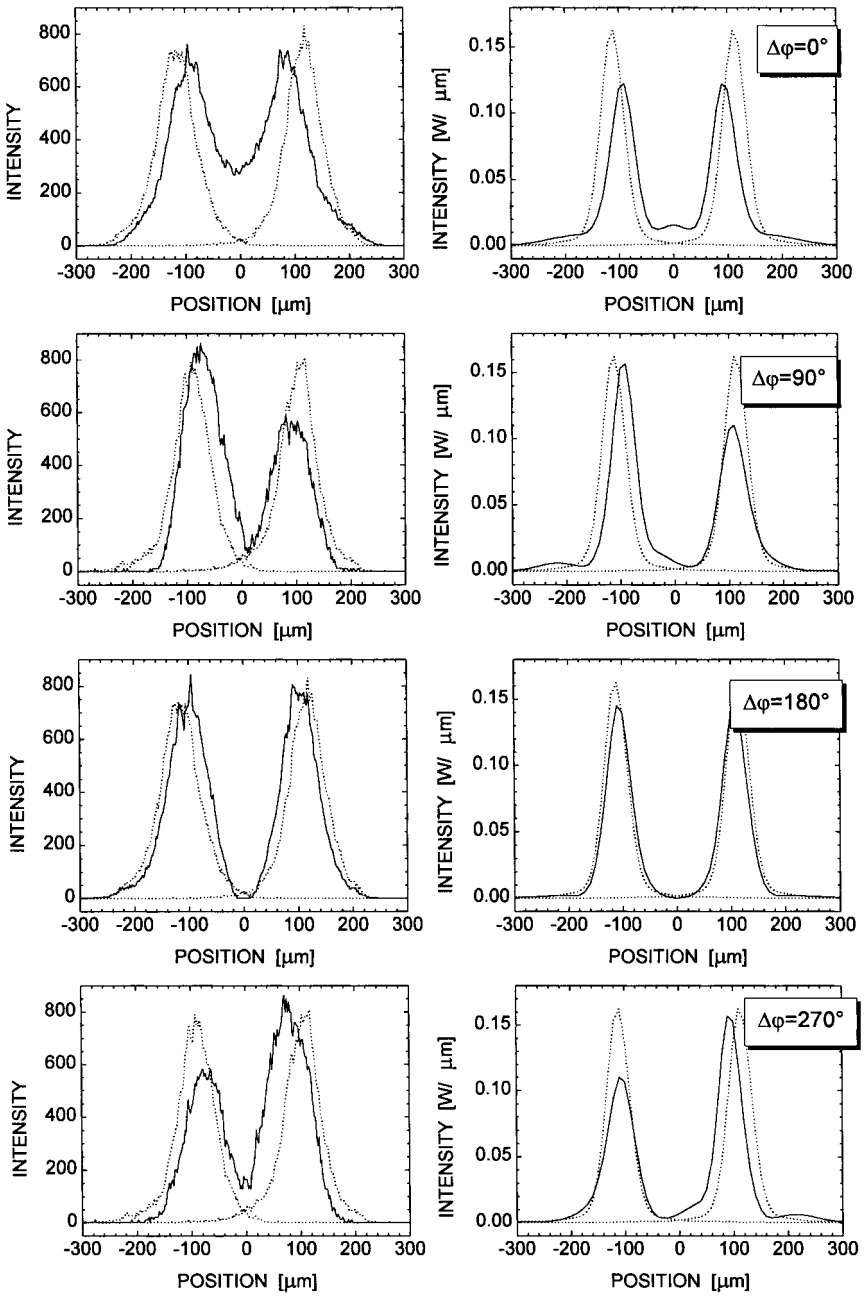

Figure 13 Output beam profiles for the two soliton interaction in the cross launching case (relative angle of 0.4°) for the large net phase mismatch of $\Delta kL \simeq 9\pi$ and different relative phase angles between the two input beams. The dotted lines show the output beams when they are launched separately (experiment: left hand side, theory: right hand side).

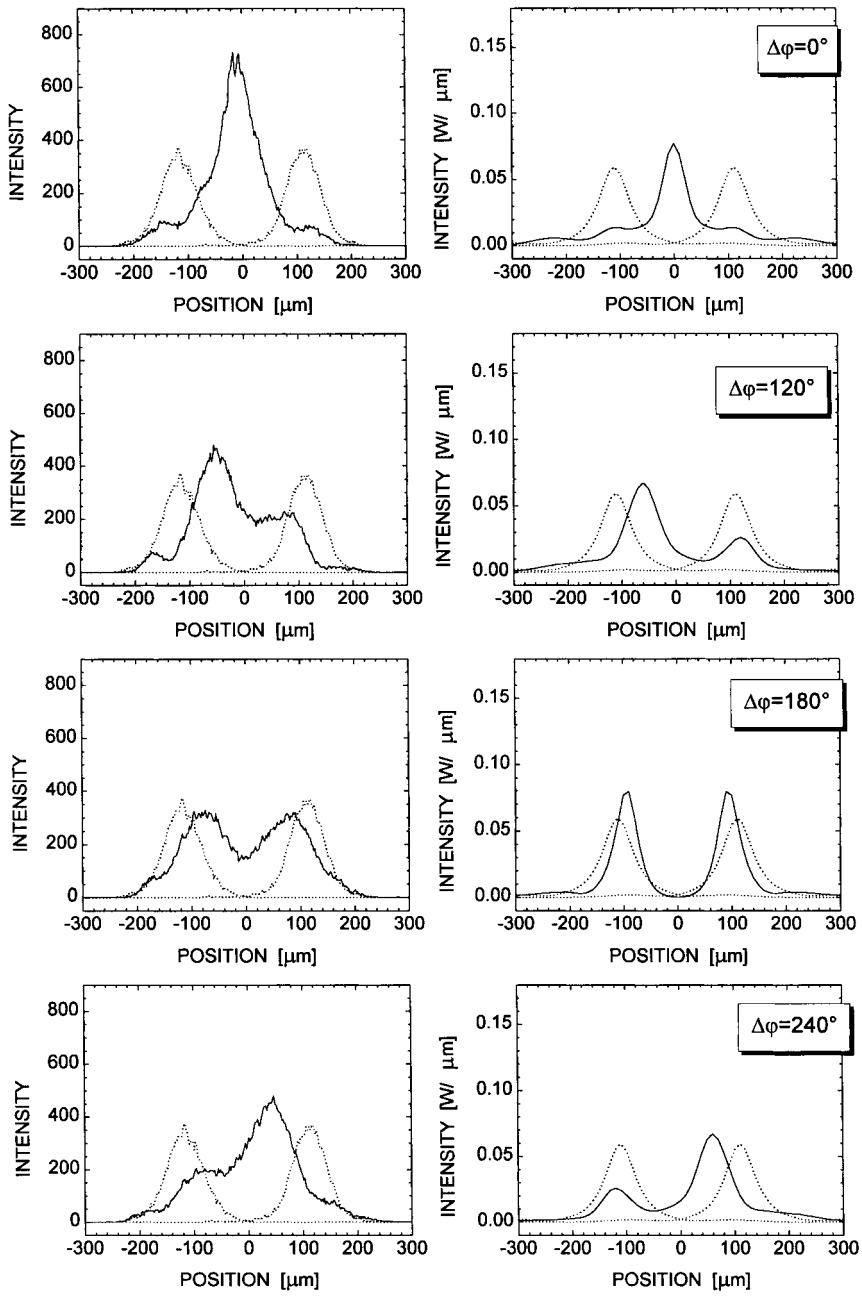

Figure 14 Output beam profiles for the two soliton interaction in the cross launching case (relative angle of 0.4°) for the small net phase mismatch of $\Delta kL \simeq 2.6\pi$ and different relative phase angles between the two input beams. The dotted lines show the output beams when they are launched separately (experiment: left hand side, theory: right hand side).

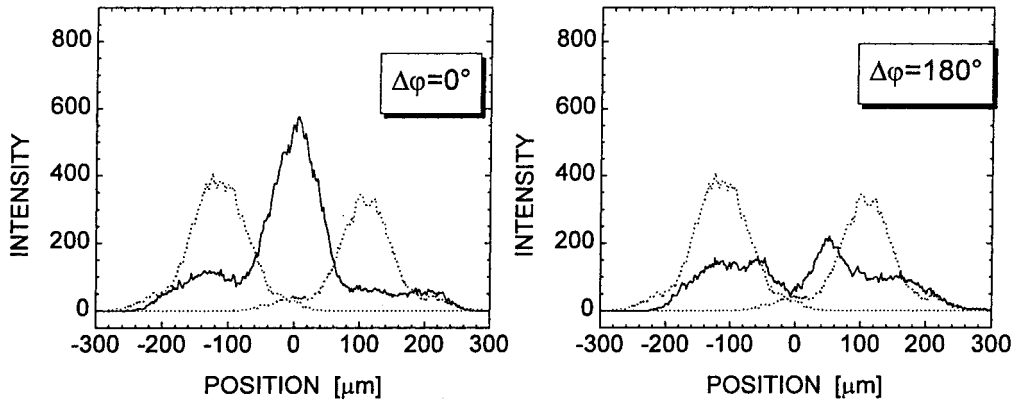

Figure 15 Measured output beam profiles for the two soliton interaction in the cross launching case (relative angle 0.4°) for the small net phase mismatch of $\Delta kL \simeq -2.4\pi$ and different relative phase angles between the two input beams. The dotted lines show the output beams when they are launched separately.

TABLE I Comparison of soliton interaction behaviour for quadratic solitons, Kerr solitons and solitons in saturable Kerr media for different relative phases $\Delta\phi$ between the solitons. The only interaction condition for which the integrable nature of the Kerr solitons leads to a unique result not shared by quadratic or saturable Kerr solitons is indicated by bold typeface in the second column

Material	$\Delta\phi = 0$	$\Delta\phi = \pi$	$\Delta\phi = \pi/2$
Case I: parallel launching			
$\chi^{(2)}\Delta kL$ large	**periodic collapse → fusion**	repulsion	repulsion + power exchange
ΔkL small	**fusion**	repulsion	repulsion + power exchange
Kerr $\chi^{(3)}$	**periodic collapse no fusion**	repulsion	repulsion + power exchange
Saturable $\chi^{(3)}$	**periodic collapse → fusion**	repulsion	repulsion + power exchange
Case II: launch at small crossing angle for $\chi^{(2)}$ ≡ parallel launch			
Case III: launch at large crossing angle			
$\chi^{(2)}$ or saturable $\chi^{(3)}$	repulsive deflection	repulsive deflection	repulsive deflection + power exchange
Kerr $\chi^{(3)}$	repulsive deflection	repulsive deflection	repulsive deflection

with simulations based on the experimental parameters. The agreement was better at the larger phase mismatches than the smaller ones, due to an increasing sensitivity of the interaction product to the spatial distribution of the wavevector mismatch for decreasing ΔkL. In these experiments only the fundamental beam was launched at the input so that the interactions were between quasi-quadratic solitons in the sense that the input beam had not yet fully evolved into a stationary soliton. Nevertheless the overall behaviour observed resembled very closely that calculated for interactions involving stationary solitons.

In the introduction it was questioned whether the interactions and collisions between quadratic solitons would resemble those known for other forms of spatial solitons. A comparison is summarized in Table I. It is clear that interactions between quadratic solitons resemble closely those in saturable Kerr media [31, 32]. This might have been expected because quadratic solitons are not solutions of integrable systems, a property they share with saturable media.

Acknowledgements

The research at CREOL was supported by DARPA, ARO and NSF. We wish to thank Dr I. Baumann for fabricating the sample.

References

1. E. INFELD and R. ROWLANDS, *Nonlinear Waves, Solitons and Chaos* (Cambridge Press, Cambridge, 1990).
2. A. C. NEWELL, *Solitons in Mathematics and Physics* (Society for Industry and Applied Mathematics, Philadelphia, 1985).
3. M. REMOISSENET, *Waves Called Solitons: Concepts and Experiments* (Springer-Verlag, Berlin, 1994).
4. J. E. BJORKHOLM and A. ASHKIN, *Phys. Rev. Lett.* **32** (1974) 129.
5. S. MANEUF and F. REYNAUD, *Opt. Commun.* **66** (1988) 325.
6. J. S. AITCHISON, A. M. WEINER, Y. SILBERBERG, M. K. OLIVER, J. L. JACKEL, D. E. A. LAIRD, E. M. VOGEL and P. W. E. SMITH, *Opt. Lett.* **15** (1990) 471.
7. J. U. KANG, G. I. STEGEMAN, A. VILLENEUVE and J. S. AITCHISON, *J. Eur. Opt. Soc., Part A Pure Appl. Opt.* **5** (1996) 583.
8. G. A. SWARTZLANDER JR, D. R. ANDERSON, J. J. REGAN, H. YIN and A. E. KAPLAN, *Phys. Rev. Lett.* **66** (1991) 1583.
9. V. TIKHONENKO, J. CHRISTOU and B. LUTHER-DAVIES, *J. Opt. Soc. Am. B* **12** (1995) 2046.
10. G. C. DUREE JR, J. L. SHULTZ, G. J. SALAMO, M. SEGEV, A. YARIV, B. CROSIGNANI, P. DI PORTO, E. J. SHARP and R. R. NEURGAONKAR, *Phys. Rev. Lett.* **71** (1993) 533.
11. M.-F. SHIH, M. SEGEV, G. C. VALLEY, G. SALAMO, B. CROSIGNANI and P. DI PORTO, *Electron. Lett.* **31** (1995) 826.
12. R. SCHIEK, Y. BAEK and G. I. STEGEMAN, *Phys. Rev. E* **53** (1996) 1138.
13. W. E. TORRUELLAS, Z. WANG, D. J. HAGAN, E. W. VANSTRYLAND, G. I. STEGEMAN, L. TORNER and C. R. MENYUK, *Phys. Rev. Lett.* **74** (1995) 5036.
14. Y. N. KARAMZIN and A. P. SUKHORUKOV, *JETP Lett.* **20** (1974) 339.
15. Y. N. KARAMZIN and A. P. SUKHORUKOV, *Zh. Eksp. Teor. Phys.* **68** (1975) 834 [*Sov. Phys.-JETP* **41** (1976) 414].
16. L. TORNER, D. MAZILU and D. MIHALACHE, *Phys. Rev. Lett.* **77** (1996) 2455.
17. M. J. WERNER and P. D. DRUMMOND, *J. Opt. Soc. Am. B* **10** (1993) 2390.
18. D. E. PELINOVSKY, A. V. BURYAK and Y. S. KIVSHAR, *Phys. Rev. Lett.* **75** (1995) 591.
19. L. TORNER, D. MIHALACHE, D. MAZILU and N. N. AKHMEDIEV, *Opt. Lett.* **20** (1995) 2183.
20. L. TORNER, *Opt. Commun.* **114** (1995) 136.
21. L. TORNER, D. MIHALACHE, D. MAZILU, E. M. WRIGHT, W. E. TORRUELLAS and G. I. STEGEMAN, *Opt. Commun.* **121** (1995) 149.
22. A. V. BURYAK, Y. S. KIVSHAR and S. TRILLO, *Phys. Rev. Lett.* **77** (1996) 5210.
23. U. PESCHEL, C. ETRICH, F. LEDERER and B. MALOMED, *Phys. Rev. E* **55** (1997) 7704.
24. R. A. FUERST, D. -M. BABOIU, B. LAWRENCE, W. E. TORRUELLAS, G. I. STEGEMAN, S. TRILLO and S. WABNITZ, *Phys. Rev. Lett.* **78** (1997) 2756.
25. W. TORRUELLAS, G. ASSANTO, B. LAWRENCE, R. A. FUERST and G. I. STEGEMAN, *Appl. Phys. Lett.* **68** (1996) 1449.
26. M. T. G. CANVA, R. A. FUERST, D. BABOIU, G. I. STEGEMAN and G. ASSANTO, *Opt. Lett.* **22** (1997) 1683.
27. R. A. FUERST, M. T. G. CANVA, D. BABOIU and G. I. STEGEMAN, *Opt. Lett.* **22** (1997) 1748.
28. S. GATZ and J. HERMANN, *IEEE J. Quantum Electron.* **28** (1992) 1732.
29. M. SHALABY, F. REYNAUD and A. BARTHELEMY, *Opt. Lett.* **17** (1992) 778.
30. J. S. AITCHISON, A. M. WEINER, Y. SILBERBERG, D. E. LEAIRD, M. K. OLIVER, J. L. JACKEL and P. W. E. SMITH, *Opt. Lett.* **16** (1991) 15.

31. M. SHIH and M. SEGEV, *Opt. Lett.* **21** (1996) 1538.
32. V. TIKHONENKO, J. CHRISTOU and B. LUTHER-DAVIES, *Phys. Rev. Lett.* **76** (1996) 2698.
33. J. U. KANG, G. I. STEGEMAN, J. S. AITCHISON and N. AKHMEDIEV, *Phys. Rev. Lett.* **76** (1996) 3699.
34. Reviewed in G. STEGEMAN, D. HAGAN and L. TORNER, *J. Opt. Quantum Electron.* **28** (1996) 1691.
35. A. V. BURYAK, Y. S. KIVSHAR and V. V. STELBINA, *Phys. Rev. A* **52** (1995) 1670.
36. D.-M. BABOIU, G. I. STEGEMAN and L. TORNER, *Opt. Lett.* **20** (1995) 2282.
37. C. ETRICH, U. PESCHEL, F. LEDERER and B. MALOMED, *Phys. Rev. A* **52** (1995) 3444.
38. D.-M. BABOIU and G. I. STEGEMAN, *J. Opt. Soc. Am. B* **14** (1997) 3143.
39. Y. BAEK, R. SCHIEK, G. I. STEGEMAN, I. BAUMANN and W. SOHLER, *Opt. Lett.* **22** (1997) 1550.
40. R. SCHIEK, *J. Opt. Soc. Am. B* **10** (1993) 1848.
41. Q. GUO, *Quantum Opt.* **5** (1993) 133.
42. R. SCHIEK, *Nonlinear Opt.* **6** (1993) 19.
43. Y. BAEK, Cascaded second order nonlinearities in lithium niobate waveguides, PhD thesis, University of Central Florida, Orlando (1997).
44. H. SEIBERT, Neue Methoden der Phasenanpassung optisch nichtlinearer Wechselwirkungen in Ti:$LiNbO_3$- und $H_xLi_{1-x}NbO_3$-Streifenwellenleitern, PhD thesis, Universität Paderborn, Paderborn, Germany (1992).
45. R. SCHIEK, H. FANG, C. G. TREVINO-PALACIOS and G. I. STEGEMAN, in Nonlinear Guided Waves and their Applications, Vol. 5 of 1998 OSA Technical Digest Series (Optical Society of America, Washington, D.C., 1998) 256.
46. R. SCHIEK, Y. BAEK and G. I. STEGEMAN, *J. Opt. Soc. Am. B* **15** (1998) 2255.
47. L. TORNER, C. R. MENYUK and G. I. STEGEMAN, *Opt. Lett.* **19** (1994) 1615.
48. C. ETRICH, U. PESCHEL, F. LEDERER, B. MALOMED and Y. KIVSHAR, *Phys. Rev. E* **54** (1996) 4321.
49. D.-M. BABOIU and G. I. STEGEMAN, *J. Opt. Quantum Electron.* **30** (1998) 849.